Supporting Information for: Closing the Gap Between Experiment and Theory: Reactive Scattering of HCl from Au(111)

Nick Gerrits*[1], Jan Geweke[2,3], Egidius W.F. Smeets[1], Johannes Voss[5], Alec M. Wodtke[2,3,4], and Geert-Jan Kroes†[1]

[1]Leiden Institute of Chemistry, Leiden University, Gorlaeus Laboratories, P.O. Box 9502, 2300 RA Leiden, The Netherlands
[2]Max Planck Institute for Biophysical Chemistry, Göttingen, Am Fassberg 11, 37077 Göttingen, Germany
[3]Institute for Physical Chemistry, University of Göttingen, Tammannstr. 6, 37077 Göttingen, Germany
[4]International Center for Advanced Studies of Energy Conversion, University of Göttingen, Tammannstr. 6, 37077 Göttingen, Germany
[5]SLAC National Accelerator Laboratory, SUNCAT Center for Interface Science & Catalysis, 2575 Sand Hill Rd, Menlo Park, California 94025, United States

S1 Convergence

Convergence of the minimum barrier height of HCl on Au(111) employing the MS-RPBEl functional is shown in Figure S1 and Table S1. Furthermore, the absolute error distribution for the training and testing data set of the HD-NNP compared to DFT calculations is shown in Figure S2. For the test set, the HD-NNP predicts for 85% of all structures energies that agree with the raw DFT data within 1 kJ/mol, 97% of all structures are within 2.5 kJ/mol of the reference data, and 98.4% of the structures reproduce the DFT energies within chemical accuracy (4.2 kJ/mol). Finally, the energy along the reaction coordinate of the minimum barrier in Figure 4 obtained with the HD-NNP is compared to the raw DFT data in Figure S3, where it is shown that the HD-NNP reproduces the raw DFT data within chemical accuracy. Since both the RMSE and Figure S2 indicate an excellent fit quality, we expect similar behavior for the other reaction coordinates.

The interlayer relaxation in this work is performed for a slab with a 1x1 surface unit cell employing an 8x8x1 k-point grid, which yields an outward interlayer relaxation of the top two layers of 3.0% for a 4 layer slab. However, calculations employing a 24x24x1 or 32x32x1 k-point grid yield an outward interlayer relaxation of 0.5% and 0.7%, respectively. DFT calculations employing the computational

*email: n.gerrits@lic.leidenuniv.nl
†email: g.j.kroes@chem.leidenuniv.nl

setup used throughout this work, but with converged interlayer distances obtained with a 24x24x1 k-point grid, suggest that both the minimum barrier and geometry are not affected significantly. For example, the barrier height is only increased by 0.2 kJ/mol. Furthermore, since experimentally a herringbone patterned surface instead of an ideal (111) surface is employed, it is possible that employing unconverged interlayer spacings might not matter for the comparison between experiment and theory. Moreover, computationally it would be untractable to redo all the calculations that have been performed for the PES. Therefore, we employ unconverged interlayer spacings throughout this work, but we also note that this should not affect results considerably.

S2 Symmetry functions

Considering that the used symmetry functions and fitting procedure have been described in earlier studies[1–5], we will only give a short summary here of the symmetry functions and their parameters[2]. As discussed in the main article, the total energy is a sum of atomic contributions that are dependent on the energetically relevant local environment, which is described by many-body atom-centered symmetry functions. This local environment is defined by the following cut-off function[2]

$$f_c(R) = \begin{cases} \frac{1}{2}\left[\cos\left(\pi \frac{R}{R_c}\right) + 1\right] & R < R_c \\ 0 & R \geq R_c, \end{cases} \tag{S1}$$

where $R_c = 11a_0$ for all symmetry functions. The radial symmetry functions are[2]

$$G_i^2 = \sum_{j \neq i} e^{-\eta(R_{i,j} - R_s)^2} f_c(R_{i,j}), \tag{S2}$$

where $R_{i,j}$ is the internuclear distance between atoms i and j, and η and R_s are parameters characterizing the function form, for which $R_s = 0$ in all cases. Furthermore, the angular symmetry functions are[2]

$$G_i^3 = 2^{1-\zeta} \sum_{j,k \neq i} (1 + \lambda \cos\theta_{i,j,k})^{\zeta} e^{-\eta(R_{i,j} + R_{i,k} + R_{j,k})} f_c(R_{i,j}) f_c(R_{i,k}) f_c(R_{j,k}), \tag{S3}$$

where $\theta_{i,j,k} = \frac{R_{i,j} \cdot R_{i,k}}{R_{i,j} R_{i,k}}$, and η, ζ and λ are parameters characterizing the function form. The parameters used for the radial and angular symmetry functions are given in Tables S2-S5, and have been generated following the procedure of Ref.[6].

S3 Site specific reactivity

The site specific reactivity of $\nu = 2, J = 1$ rovibrationally excited HCl is compared to results where the rovibrational population of HCl is sampled according to a Boltzmann distribution according to the nozzle temperature in Figure S4. For $\nu = 2, J = 1$ rovibrationally excited HCl a statistical site specific reactivity is obtained for $S_0 > 0.2$, whereas for $S_0 < 0.2$ the site specific reactivity is non-statistical. As discussed in the main work, we conclude here that adding vibrational energy increases the dynamical accessibility of specific barriers, especially that of the top site.

S4 Vibrational excitation probabilities

The scattering angle dependence of the vibrational excitation probabilities of HCl is shown in Figure S5. The vibrational transition probabilities ($T_{\nu=1,j=1\rightarrow\nu=2}$) are increased by a factor 1.2 for low incidence energy up to a factor 2.3 for high incidence energy, when only a range of scattering angles is considered relative to all scattering angles. The increase in transition probabilities also results in a larger discrepancy between experiment and theory. However, as discussed in the main work, the experimental correction for the use of a specific scattering angle is likely to be accurate, and therefore including all scattering angles in the theoretical analysis should be adequate.

The beam parameters of Ref.[7] have not been published previously. We have included the beam parameters of the new experiments presented in Ref.[7] in Table S6 for future reference, but note that these parameters have not been employed in this work. The velocity distributions of Ref.[7] are somewhat broader than the ones simulated in this work. Nevertheless, as can be seen from Figure S6, the transition probability does not depend considerably on the width of the velocity distribution.

S5 Elbow plots

Figure S7 shows an elbow plot of the minimum TS, which is also shown in Figure 4. The white dashed lines are drawn from the top right corner, where the lowest energy along these lines yields the MEP.

The barrier height as a function of θ and ϕ (the polar and azimuthal angles, respectively) for the high symmetry sites and the minimum barrier impact site is shown in Figure S8. The top site seems to be narrow, especially for the θ angle, while the bridge site seems to be mainly narrow in the ϕ angle. The fcc site (which is similar to the hcp site) is neither. Finally, for the minimum barrier it seems that the orientation in the XY plane (i.e., ϕ) is extremely important, which would also reduce the overall reactivity near the top site.

References

(1) Behler, J.; Parrinello, M. Generalized Neural-Network Representation of High-Dimensional Potential-Energy Surfaces. *Phys. Rev. Lett.* **2007**, *98*, 146401.

(2) Behler, J. Atom-Centered Symmetry Functions for Constructing High-Dimensional Neural Network Potentials. *J. Chem. Phys.* **2011**, *134*, 074106.

(3) Behler, J. Representing Potential Energy Surfaces by High-Dimensional Neural Network Potentials. *J. Phys.: Condens. Matter* **2014**, *26*, 183001.

(4) Shakouri, K.; Behler, J.; Meyer, J.; Kroes, G.-J. Accurate Neural Network Description of Surface Phonons in Reactive Gas–Surface Dynamics: N_2 + Ru(0001). *J. Phys. Chem. Lett.* **2017**, *8*, 2131–2136.

(5) Shakouri, K.; Behler, J.; Meyer, J.; Kroes, G.-J. Analysis of Energy Dissipation Channels in a Benchmark System of Activated Dissociation: N_2 on Ru(0001). *J. Phys. Chem. C* **2018**, *122*, 23470–23480.

(6) Gastegger, M.; Schwiedrzik, L.; Bittermann, M.; Berzsenyi, F.; Marquetand, P. wACSF—Weighted Atom-Centered Symmetry Functions as Descriptors in Machine Learning Potentials. *J. Chem. Phys.* **2018**, *148*, 241709.

(7) Geweke, J.; Shirhatti, P. R.; Rahinov, I.; Bartels, C.; Wodtke, A. M. Vibrational Energy Transfer near a Dissociative Adsorption Transition State: State-to-State Study of HCl Collisions at Au(111). *J. Chem. Phys.* **2016**, *145*, 054709.

(8) Rahinov, I.; Cooper, R.; Yuan, C.; Yang, X.; Auerbach, D. J.; Wodtke, A. M. Efficient Vibrational and Translational Excitations of a Solid Metal Surface: State-to-State Time-of-Flight Measurements of HCl(ν=2,J=1) Scattering from Au(111). *J. Chem. Phys.* **2008**, *129*, 214708.

(9) Ran, Q.; Matsiev, D.; Auerbach, D. J.; Wodtke, A. M. Observation of a Change of Vibrational Excitation Mechanism with Surface Temperature: HCl Collisions with Au(111). *Phys. Rev. Lett.* **2007**, *98*, 237601.

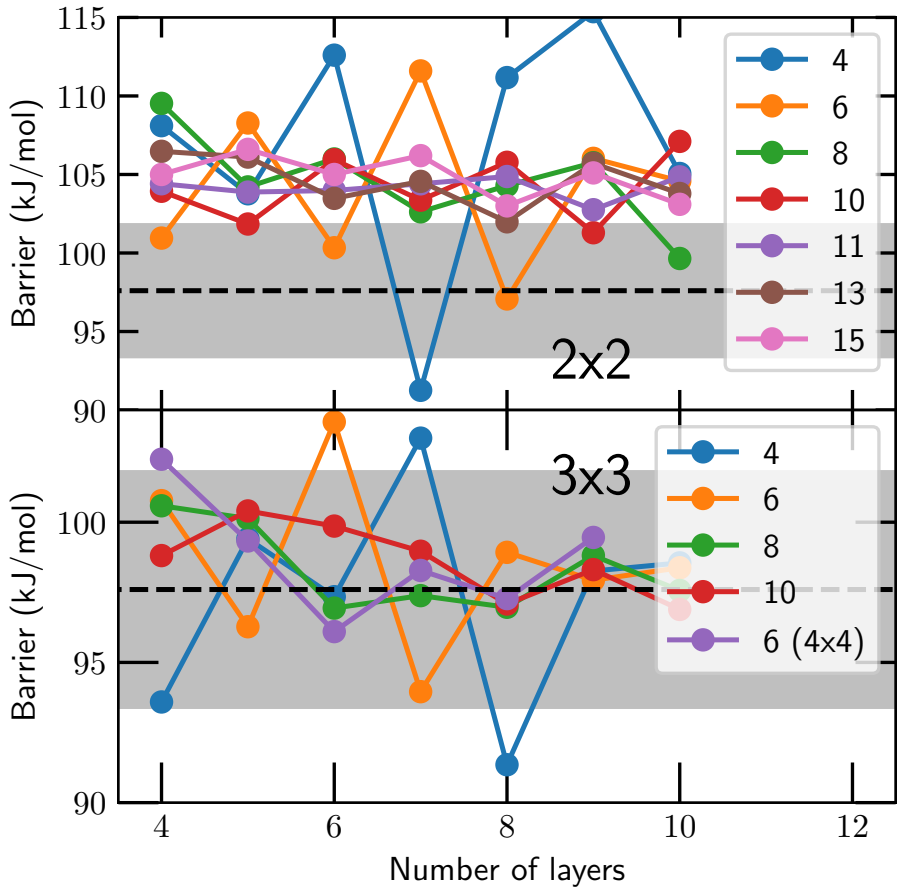

Figure S1: Convergence of the minimum barrier height (kJ/mol) of HCl on Au(111) as a function of the amount of layers and k-points using the MS-RPBEl functional. The first panel and second panel used a 2x2 and 3x3 supercell, respectively. The second panel also includes the convergence for a 4x4 supercell using a 6x6x1 k-point grid. The dashed lines indicate the converged barrier height. The calculations of the PES were done with a 3x3 surface unit cell, 4 layers, and an 8x8x1 k-point grid.

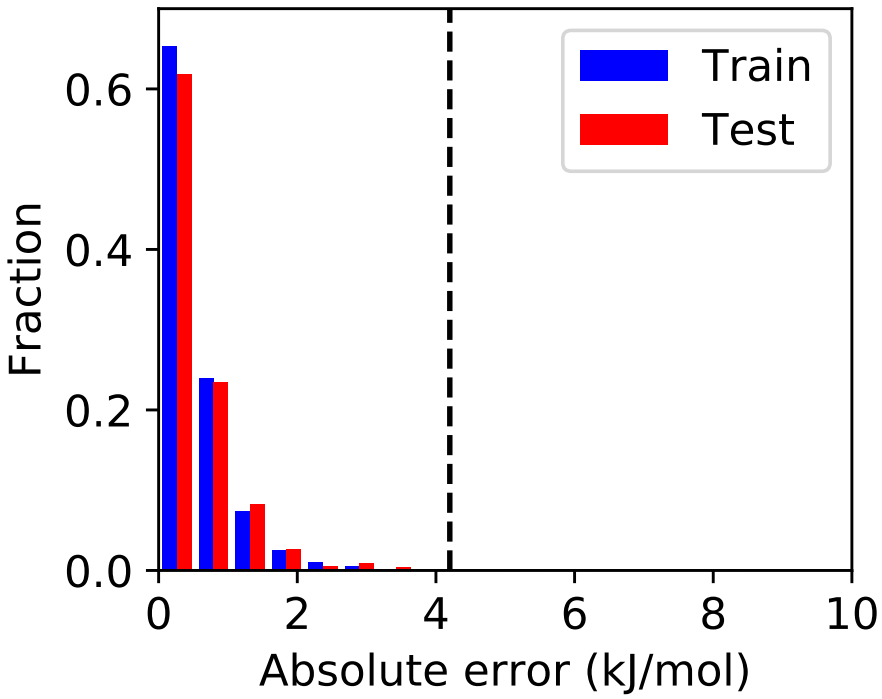

Figure S2: Distribution of absolute total energy errors (kJ/mol) of the HD-NNP compared to the DFT total energy. Blue indicates the training set, whereas red indicates the test set. The dashed line indicates chemical accuracy, i.e., 4.2 kJ/mol.

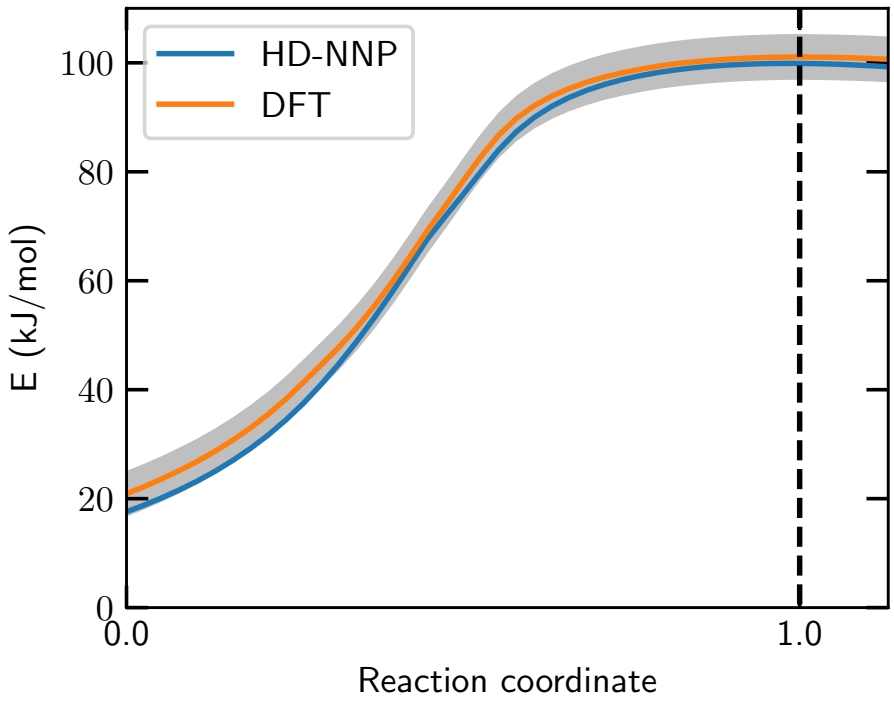

Figure S3: Energy along the reaction coordinate of the minimum barrier's MEP (as defined in Figure 4) obtained from the HD-NNP and raw DFT data. The reaction coordinate value of zero is taken to be HCl with $Z_{\mathrm{Cl}} = 3\,\text{Å}$, and the value of one is the TS. The grey area indicates chemical accuracy (i.e., 4.2 kJ/mol) and the dashed black line indicates the TS.

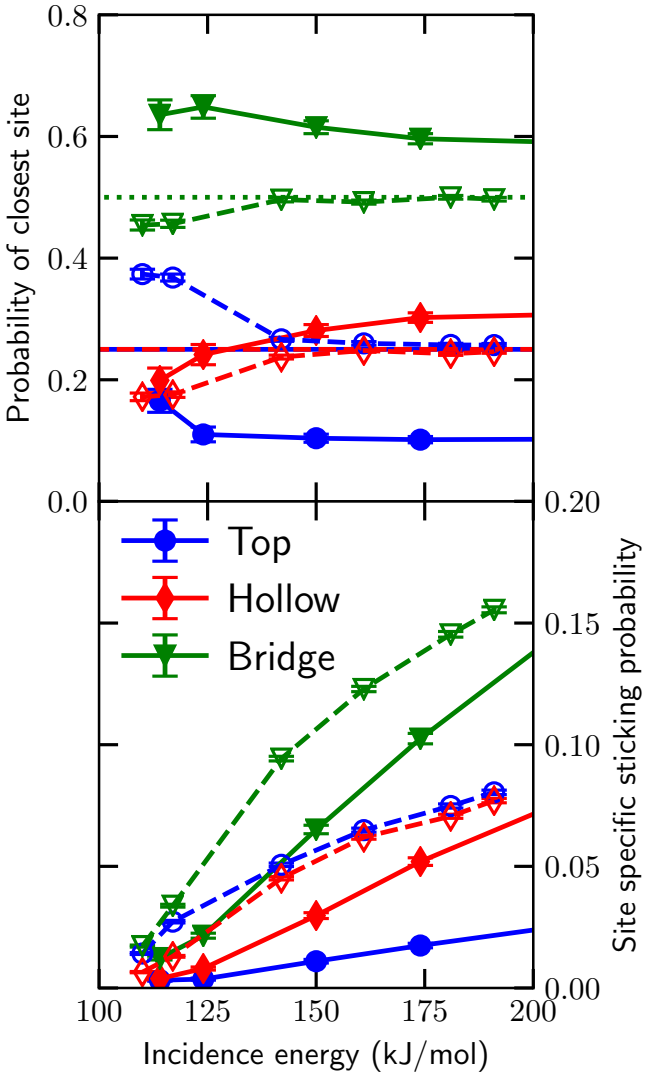

Figure S4: (a) Fractions of the closest high symmetry sites encountered by HCl, i.e., the top, hollow, and bridge (blue, red, and green, respectively) sites, as a function of the incidence energy at the time of dissociation, i.e., when $r = r^{\ddagger}$. The dashed and dotted lines indicate the statistical average for the high symmetry sites. The open and solid symbols indicate the use of a rovibrational population of only $\nu = 2, J = 1$ and according to a Boltzmann distribution, respectively. The $\nu = 2, J = 1$ state selected HCl results are shifted by 66 kJ/mol (i.e., the energy difference between $\nu = 0, J = 0$ and $\nu = 2, J = 1$) in order to compare to the results where the vibrational population of HCl is sampled with a Boltzmann distribution according to the nozzle temperature. (b) Sticking probability of HCl on the high symmetry sites as a function of the incidence energy. Note that the site specific sticking probabilities add up to the total sticking probability. The error bars represent 68% confidence intervals.

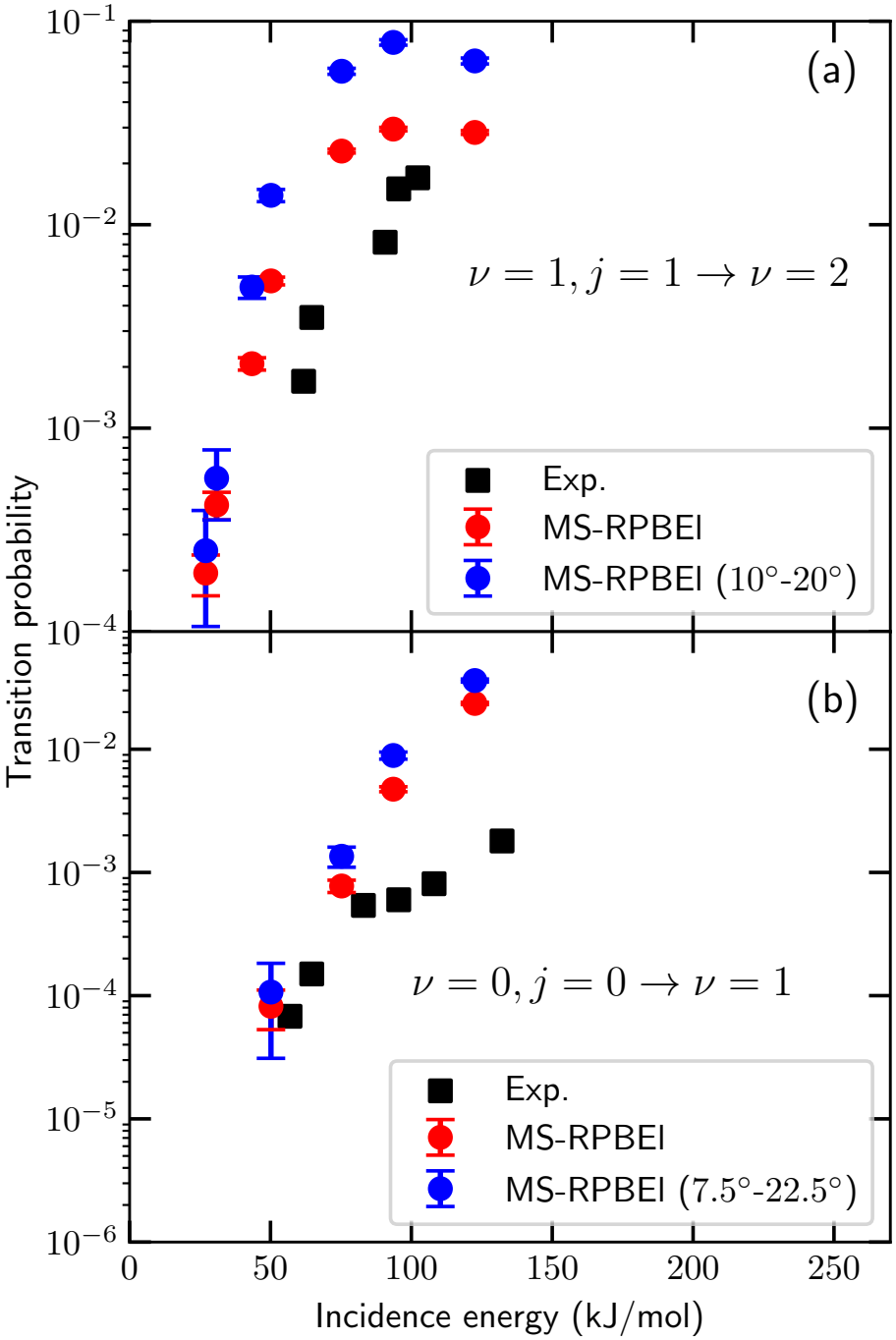

Figure S5: (Vibrational excitation probability of HCl scattered from Au(111) (T_S = 170 K) using the MS-RPBEl functional for $\nu = 1, j = 1 \rightarrow \nu = 2$ (a) and $\nu = 0, j = 0 \rightarrow \nu = 1$ (b). Experimental results from Ref.[7] are indicate by the black squares. Computed results with the MS-RPBEl functional including all scattering angles or only in the range of 10° to 20° (a) or 7.5° to 22.5° (b) are indicated by the red and blue circles, respectively.

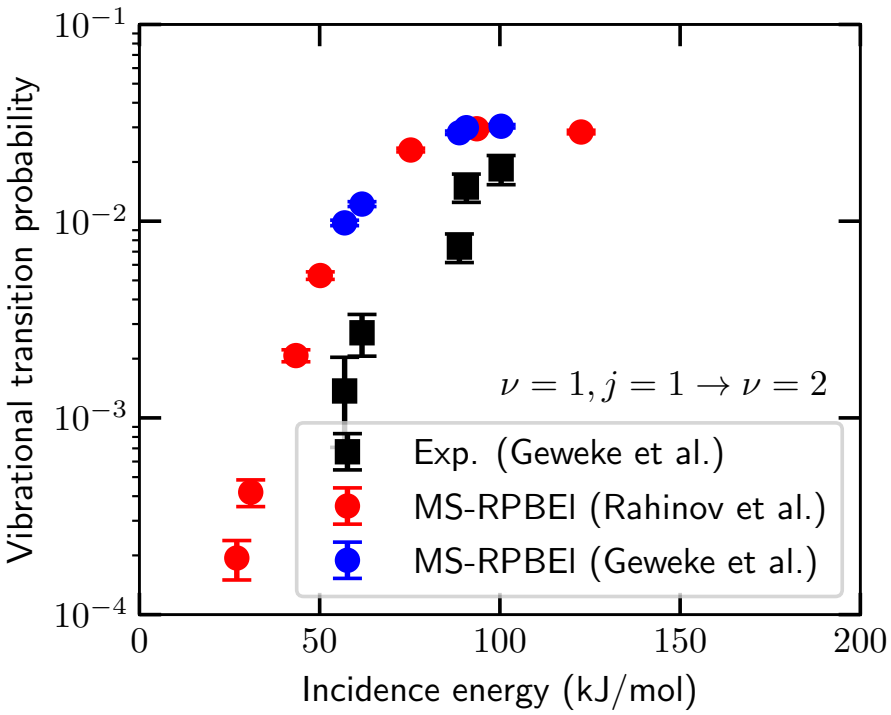

Figure S6: Vibrational excitation probability of HCl scattered from Au(111) (T_S = 170 K) using the MS-RPBEl functional for $\nu = 1, j = 1 \rightarrow \nu = 2$. Experimental results from Ref.[7] are indicated by the black squares. Computed results with the MS-RPBEl functional employing beam parameters from Refs.[8] (which are employed in Figure 9) and[7] are indicated by the red and blue circles, respectively.

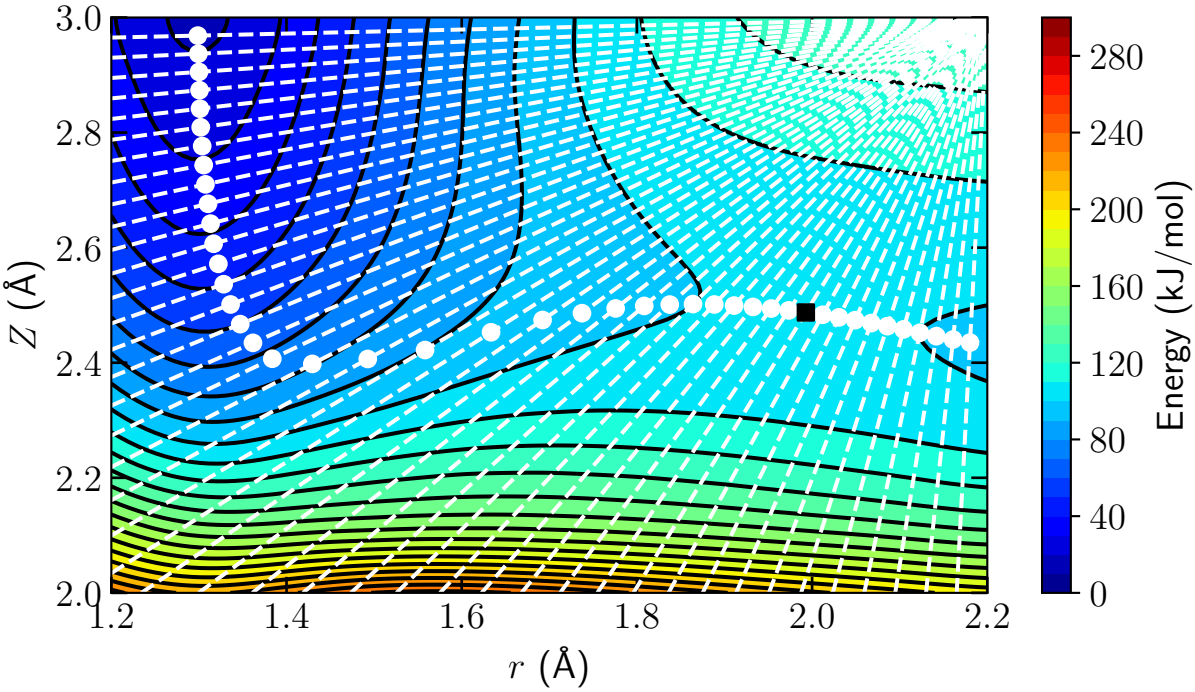

Figure S7: Elbow plot of HCl on Au(111) as a function of Z_{Cl} and r using the MS-RPBEl functional for the minimum TS. All other degrees of freedom are relaxed. Black contour lines are drawn at an interval of 10 kJ/mol between 0 and 200 kJ/mol. The white circles indicate the MEP in reduced dimensionality and the black square indicates the highest point along the MEP. The white dashed lines indicate the lines from which the MEP is determined.

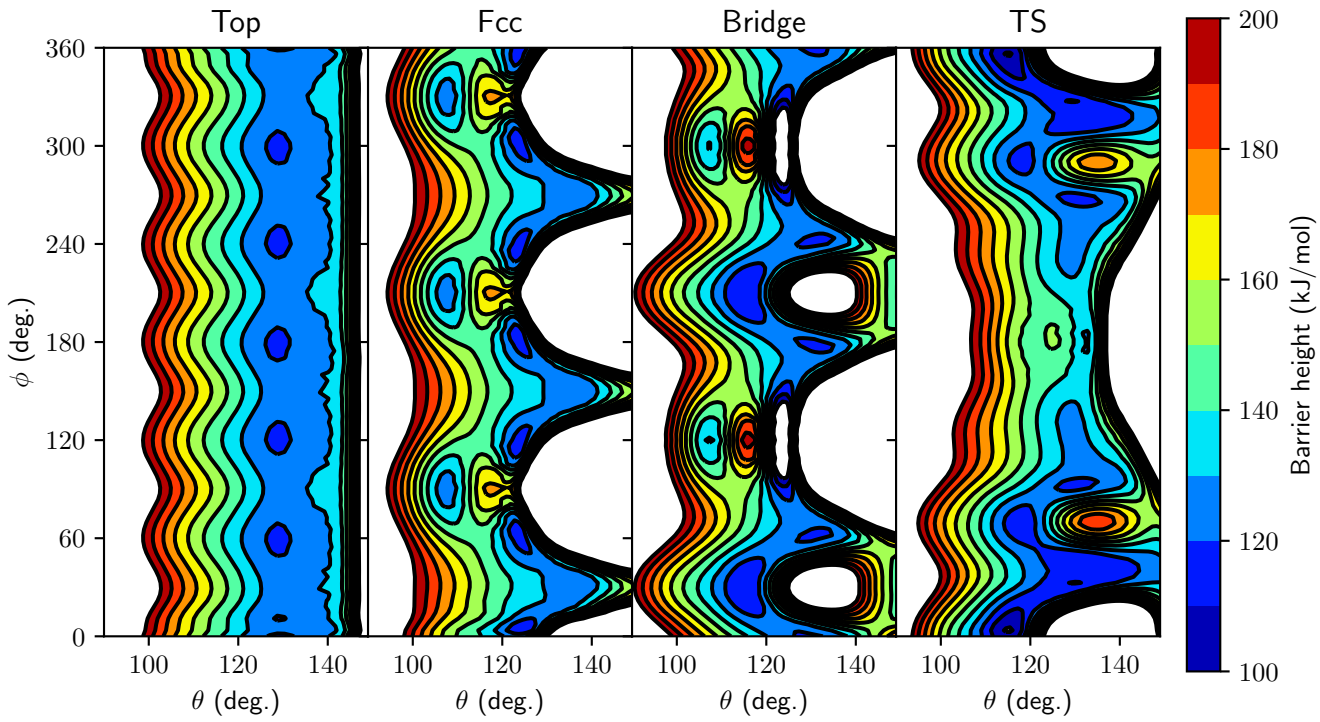

Figure S8: Barrier height of HCl on Au(111) as a function of the θ and ϕ angles for the top, fcc and bridge sites, and the minimum TS. The black contour lines are drawn at a interval of 10 kJ/mol from 100 to 200 kJ/mol.

Table S1: Same as Figure S1. The results obtained with the employed computational set up in the DFT calculations for the training data set is in bold and the most converged result (i.e., obtained with the largest setup) is in italic.

Layers	k-points	E_b, 2x2	E_b, 3x3
4	4x4x1	108.1	93.6
4	6x6x1	101.0	100.8
4	8x8x1	109.5	**100.6**
4	10x10x1	103.9	98.8
4	11x11x1	104.4	
4	13x13x1	106.5	
4	15x15x1	105.0	
5	4x4x1	103.8	99.4
5	6x6x1	108.3	96.3
5	8x8x1	104.2	100.1
5	10x10x1	101.8	100.4
5	11x11x1	103.9	
5	13x13x1	106.1	
5	15x15x1	106.6	
6	4x4x1	112.6	97.3
6	6x6x1	100.3	103.6
6	8x8x1	106.0	96.9
6	10x10x1	105.9	99.9
6	11x11x1	104.0	
6	13x13x1	103.5	
6	15x15x1	105.0	
7	4x4x1	91.3	103.0
7	6x6x1	111.6	94.0
7	8x8x1	102.6	97.4
7	10x10x1	103.4	99.0
7	11x11x1	104.4	
7	13x13x1	104.6	
7	15x15x1	106.2	
8	4x4x1	111.2	91.4
8	6x6x1	97.1	98.9
8	8x8x1	104.3	97.0
8	10x10x1	105.8	97.1
8	11x11x1	104.9	
8	13x13x1	102.0	
8	15x15x1	103.0	
9	4x4x1	115.4	98.3
9	6x6x1	106.0	97.9
9	8x8x1	105.7	98.8
9	10x10x1	101.3	98.3
9	11x11x1	102.8	
9	13x13x1	105.7	
9	15x15x1	105.1	
10	4x4x1	105.1	98.5
10	6x6x1	104.6	98.4
10	8x8x1	99.6	97.6
10	10x10x1	107.1	*96.9*
10	11x11x1	104.9	
10	13x13x1	103.8	
10	15x15x1	103.1	

Table S2: The parameters used for the radial symmetry functions describing the interaction of Cl as a reference atom with its neighbouring atoms within the cut-off radius.

Reference atom type	Neighbouring atom type	η
Cl	H	0.00453515
Cl	H	0.00598145
Cl	H	0.00824846
Cl	H	0.01209877
Cl	H	0.01944059
Cl	H	0.0362426
Cl	H	0.08999082
Cl	H	0.5
Cl	Au	0.00453515
Cl	Au	0.00598145
Cl	Au	0.00824846
Cl	Au	0.01209877
Cl	Au	0.01944059
Cl	Au	0.0362426
Cl	Au	0.08999082
Cl	Au	0.5

Table S3: Same as Table S2 but with H as the reference atom.

Reference atom type	Neighbouring atom type	η
H	Cl	0.00453515
H	Cl	0.00598145
H	Cl	0.00824846
H	Cl	0.01209877
H	Cl	0.01944059
H	Cl	0.0362426
H	Cl	0.08999082
H	Cl	0.5
H	Au	0.00453515
H	Au	0.00598145
H	Au	0.00824846
H	Au	0.01209877
H	Au	0.01944059
H	Au	0.0362426
H	Au	0.08999082
H	Au	0.5

Table S4: Same as Table S2 but with Au as the reference atom.

Reference atom type	Neighbouring atom type	η
Au	Cl	0.00453515
Au	Cl	0.00598145
Au	Cl	0.00824846
Au	Cl	0.01209877
Au	Cl	0.01944059
Au	Cl	0.0362426
Au	Cl	0.08999082
Au	Cl	0.5
Au	H	0.00453515
Au	H	0.00598145
Au	H	0.00824846
Au	H	0.01209877
Au	H	0.01944059
Au	H	0.0362426
Au	H	0.08999082
Au	H	0.5
Au	Au	0.00453515
Au	Au	0.00593499
Au	Au	0.00809917
Au	Au	0.01170534
Au	Au	0.01838994
Au	Au	0.03299386
Au	Au	0.07561728
Au	Au	0.32

Table S5: The parameters used for the angular symmetry functions describing the interaction of a reference atom with its neighbouring atoms within the cut-off radius.

η	λ	ζ
0.00453514739	1	1
0.00929752066	1	1
0.02880000000	1	1
0.00453514739	1	4
0.00929752066	1	4
0.02880000000	1	4
0.00453514739	-1	1
0.00929752066	-1	1
0.02880000000	-1	1
0.00453514739	-1	4
0.00929752066	-1	4
0.02880000000	-1	4

Table S6: Beam parameters from Ref.[7] that describe the experimental HCl velocity distributions. The stream energy E_0, stream velocity v_0, and width parameter α are determined through time-of-flight measurements. Note that only in the case of the $\nu = 1 \rightarrow 2$ excitation experiments (Figure 9a) all of these incident conditions were employed, whereas in the $\nu = 0 \rightarrow 1$ experiments (Figure 9b) only $\langle E_\mathrm{i} \rangle = 62\,\mathrm{kJ/mol}$ and $\langle E_\mathrm{i} \rangle = 91\,\mathrm{kJ/mol}$ were employed. The remaining experimental data points in Figure 9b were taken from Ref.[9], where only the mean incidence energy was provided.

$\langle E_\mathrm{i} \rangle$ (kJ/mol)	E_0 (kJ/mol)	v_0 (m/s)	α (m/s)
57	57	1765	101
62	61	1831	95
89	87	2190	150
91	90	2226	110
100	100	2343	136